# Supporting Information

## Transparent, flexible, and stretchable $WS_2$ based humidity sensors for electronic skin

Huayang Guo[1], Changyong Lan[1], Zhifei Zhou[1], Peihua Sun[1], Dapeng Wei[2], and Chun Li[1*]

[1]State Key Laboratory of Electronic Thin Films and Integrated Devices, and School of Optoelectronic Information, University of Electronic Science and Technology of China No.4, Section 2, North Jianshe Road, Chengdu, 610054, China

[2]Chongqing Institute of Green and Intelligent Technology, Chinese Academy of Sciences Fangzheng Avenue, Shuitu Hi-tech Industrial Park, 400714, China

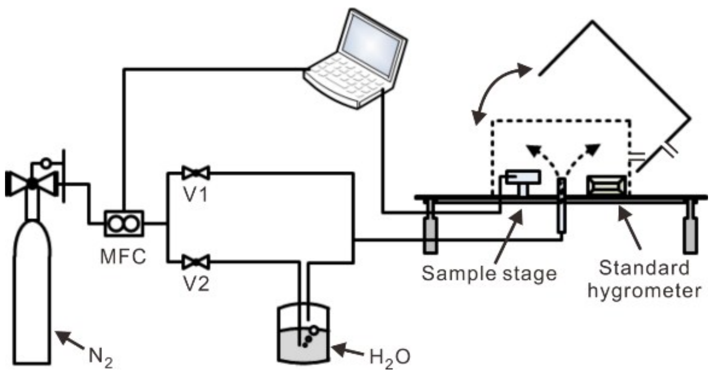


**Figure S1.** Schematic illustration of the humidity measurement system. In order to increase the RH level gradually, we first open valve V1 but close valve V2 so that the residual mositure gas can be exhausted by the pure $N_2$ gas. Then we close valve V1 but open valve V2. The RH level will increase because water molecules will get into the chamber with flowing $N_2$ gas. During the process, the RH level can be monitor by the standard hygrometer. For the time-dependent sensing performance test, we exposed the sensor to air by instantly opening the chamber lid and closing the lid following with rapid moisture injection. In this way, the humidity can be changed quickly.

* Author to whom any correspondence should be addressed. E-mail: lichun@uestc.edu.cn

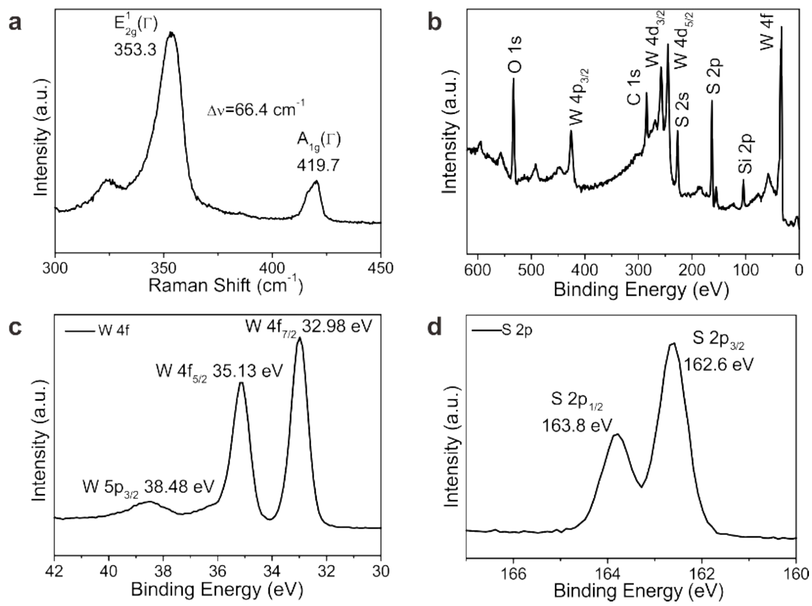


**Figure S2.** (a) Raman spectrum of the as-synthesized $WS_2$ film. $WS_2$ characteristic Raman peaks of the $E^1_{2g}$ and $A_{1g}$ phonon modes locates at 353.3 and 419.7 cm$^{-1}$, respectively. The difference between the two modes is about 66.4 cm$^{-1}$, further confirming multilayer feature of the as-synthesized $WS_2$. (b) XPS survey spectrum of $WS_2$ sample. Full scan spectrum shows that except the main peaks of W and S, Si signal from the substrate was also observed, suggesting the $WS_2$ film is thin enough to allow escape of photoelectrons originating from substrate. (c) XPS scan for W. The detailed W 4*f* scan reveals two peaks, attributed to doublet W $4f_{7/2}$ and W $4f_{5/2}$, are located at 32.98 and 35.13 eV, respectively. (d) XPS scan for S. The detailed S 2*p* scan also shows two peaks, corresponding to S $2p_{3/2}$ and S $2p_{1/2}$ orbital of divalent sulfide ions, are observed at 162.6 and 163.8 eV, respectively.

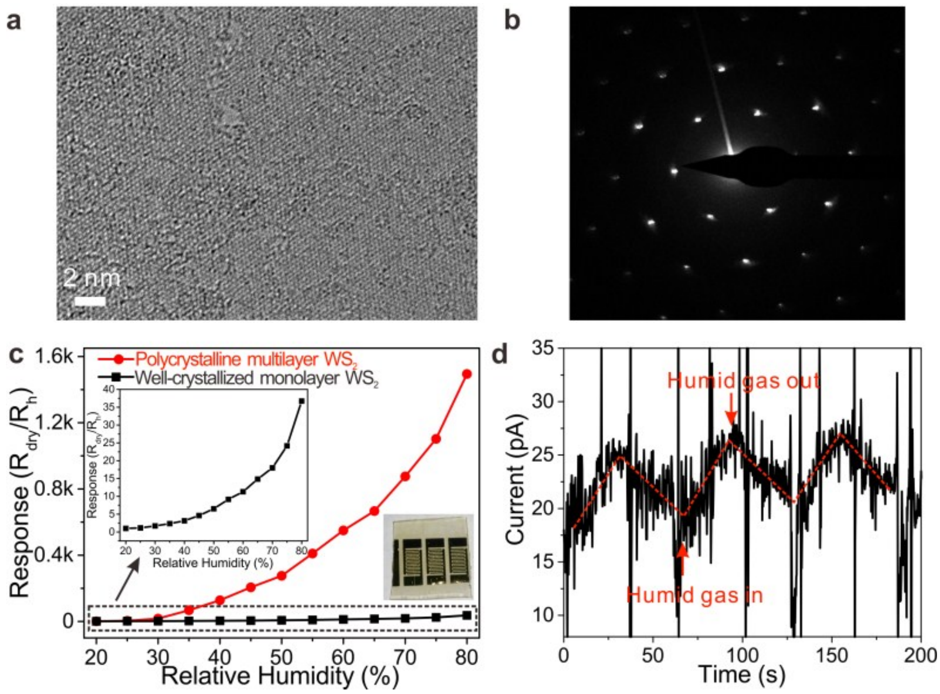


**Figure S3.** Structural characterization and sensing performance of the CVD-grown well-crystallized $WS_2$. (a) HRTEM of the well-crystallized $WS_2$. Lattice fringes can be clearly seen. (b) SAED of the as-grown $WS_2$ sample, which suggest the high quality of the $WS_2$ sample. (c) Responses of the well-crystallized $WS_2$ and polycrystal $WS_2$ in different relative humidity, respectively. Top inset: magnified curve of the well-crystallized $WS_2$. Bottom inset: photo image of the as-fabricated sensor. It is obvious that the well-crystallized $WS_2$ has poor humidity sensing performance compared with the sulfurization-grown polycrystalline $WS_2$ sample. (d) Dynamic response of the well-crystallized $WS_2$ to humid gas between 35% and 40% RH. Red dash line indicates the trend of sensor's response to humid gas. The signals are mostly submerged by noise.

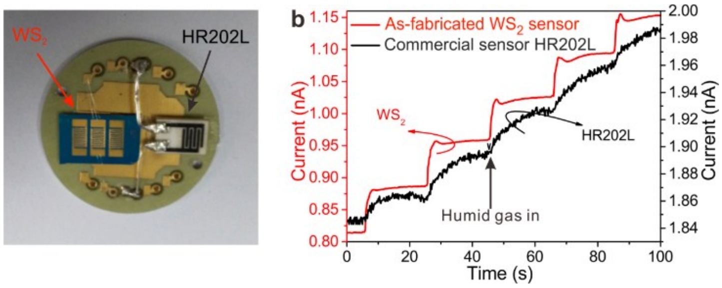


**Figure S4.** Comparision of humidity sensing performance between the fabricated $WS_2$ gas sensor and a comericial avaible humidiy sensor (AOSONG Mod. HR202L)**.** (a) Photo image and (b) humid gas response of a $WS_2$ humidity sensor and a commercial humidity sensor contacted to a testing stage.

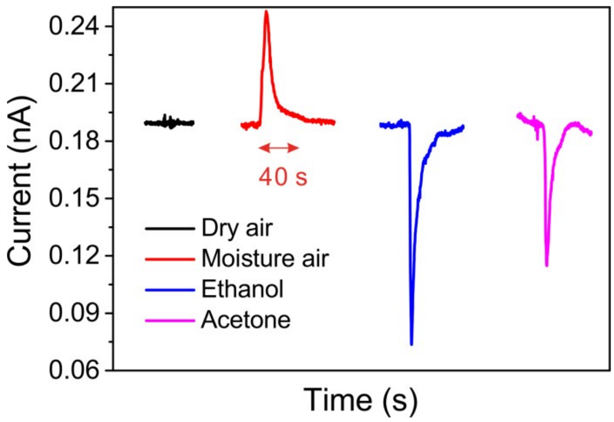


**Figure S5.** Comparision of the device sensing response to different gases. Clearly, the $WS_2$ film shows current increase response to water mositure, while it shows current decrease response to ethanoal and acetone, and no observable current response to dry dair.

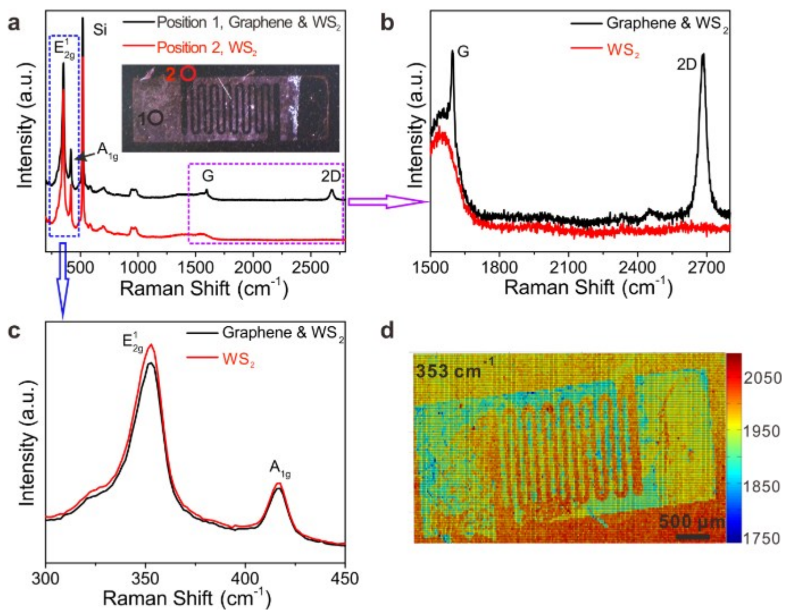


**Figure S6.** Raman characterization of the as-fabricated transparent humidity sensor with graphene IDEs attached onto $WS_2$ film. (a) Raman spectrum of the graphene IDE/$WS_2$ film. The black line belongs to the area with graphene attached onto $WS_2$ thin film. The red line belongs to the $WS_2$ area only. (b) Enlarged spectrum of high wavenumber region shown in (a). The G band and 2D band of graphene can be clearly seen. (c) Enlarged spectrum of low wavenumber region shown in (a). Because of the graphene attached onto $WS_2$ film, the intensity of $E_{2g}^{1}$ and $A_{1g}$ band of the $WS_2$ with graphene attaching is slightly small than that of pure $WS_2$ film only. (d) Raman mapping of the device. The mapping is formed by recording the intensity of the $E_{2g}^{1}$ band of $WS_2$. Clearly, the region with graphene IDEs covering shows lower Raman intensity than that of $WS_2$ film without graphene covering.

**Table S1**. Sensing performance of the reported humidity sensors based on 2D materials.

| Material | Sensitivity | $t_{res}$ | $t_{rec}$ | ΔR |
|---|---|---|---|---|
| Graphene[1] | $S(50\%)=\left\|\frac{\Delta R}{R_0}\right\| \approx 0.9\%$ | NA | NA | NA |
| GO[2] | NA | 30 ms | 30 ms | ↘ |
| $MoS_2$/GO[3] | $S(85\%)=\frac{I_{humidity}}{I_{baseline}}=1600$ | 43 s | 37 s | ↘ |
| $MoS_2$[4] | $S(84\%)=\frac{R(84\%)}{R(11\%)}\approx 7.5$ | >500 s | >2000 s | ↗ |
| $MoS_2$[5] | $S(60\%)=\frac{R_{60\%}-R_0}{R_0}\times 100\% \approx 130\%$ | 9 s | 17 s | ↗ |
| $MoS_2$[6] | $S(60\%)=\frac{R_H}{R_D}\approx 3$ | 9 s | 17 s | ↗ |
| $MoS_2$[7] | $S(95\%)=\frac{R_{RH}}{R_{dry}}\approx 14$ | NA | NA | ↗ |
| $VS_2$[8] | $S=\frac{R_{RH}}{R_{dry}}=30$ | 30-40 s | 12-50 s | ↗ |
| black phosphorus[9] | $S(97\%)=\frac{R_{11\%}-R_{RH}}{R_{RH}}\times 100\% \approx 521\%$ | 101 s | 26 s | ↘ |
| $WS_2$[10] | $S(80\%)=\frac{I_{80\%}}{I_{25\%}}=37.5$ | 13 s | 17 s | ↘ |
| $WS_2$[11] | $S(97.3\%)=\frac{R_{11\%}-R_{97.3\%}}{R_{97.3\%}}\times 100\% \approx 469\%$ | 12 s | 13 s | ↘ |
| $WS_2$ (our work) | $S(90\%)=\frac{R_{20\%}}{R_{90\%}}\approx 2357$ | 5s | 6s | ↘ |

**Refrences**


1. Y. H. Kim, S. J. Kim, Y.-J. Kim, Y.-S. Shim, S. Y. Kim, B. H. Hong and H. W. Jang, *ACS Nano*, 2015, **9**, 10453-10460.
2. S. Borini, R. White, D. Wei, M. Astley, S. Haque, E. Spigone, N. Harris, J. Kivioja and T. Ryhanen, *ACS Nano*, 2013, **7**, 11166-11173.
3. D. Burman, R. Ghosh, S. Santra and P. Guha, *RSC Adv.*, 2016.
4. D. J. Late, Y. K. Huang, B. Liu, J. Acharya, S. N. Shirodkar, J. Luo, A. Yan, D. Charles, U. V. Waghmare, V. P. Dravid and C. N. Rao, *ACS Nano*, 2013, **7**, 4879-4891.
5. S.-L. Zhang, H. Jung, J.-S. Huh, J.-B. Yu and W.-C. Yang, *J. Nanosci. Nanotechnol.*, 2014, **14**, 8518-8522.
6. S.-L. Zhang, H.-H. Choi, H.-Y. Yue and W.-C. Yang, *Curr. Appl. Phys.*, 2014, **14**, 264-268.

7. C. Ahn, J. Lee, H. U. Kim, H. Bark, M. Jeon, G. H. Ryu, Z. Lee, G. Y. Yeom, K. Kim and J. Jung, *Adv. Mater.*, 2015, **27**, 5223-5229.
8. J. Feng, L. Peng, C. Wu, X. Sun, S. Hu, C. Lin, J. Dai, J. Yang and Y. Xie, *Adv. Mater.*, 2012, **24**, 1969-1974.
9. M. B. Erande, M. S. Pawar and D. J. Late, *ACS Appl. Mat. Interfaces*, 2016, **8**, 11548-11556.
10. R. K. Jha and P. K. Guha, *Nanotechnology*, 2016, **27**, 475503.
11. A. S. Pawbake, R. G. Waykar, D. J. Late and S. R. Jadkar, *ACS Appl. Mat. Interfaces*, 2016, **8**, 3359-3365.